A&A 388, 652–659 (2002)
DOI: 10.1051/0004-6361:20020502

Astronomy & Astrophysics

Unveiling the structure of the planetary nebula M 2-48:

Kinematics and physical conditions

L. López-Martín[1,2], J. A. López[3], C. Esteban[1], R. Vázquez[3], A. Raga[4], J. M. Torrelles[5], L. F. Miranda[6], J. Meaburn[7], and L. Olguín[8]

[1] Instituto de Astrofísica de Canarias, c/Vía Láctea s/n, 38200 La Laguna, Tenerife, Spain
e-mail: luislm,cel@ll.iac.es
[2] Observatoire de Paris, DEMIRM, UMR 8540 du CNRS, 61 avenue de l'Observatoire, 75014 Paris, France
[3] Instituto de Astronomía, UNAM, Km 103, Carretera Tijuana-Ensenada, 22860 Ensenada, B.C., Mexico
e-mail: jal,vazquez@astrosen.unam.mx
[4] Instituto de Ciencias Nucleares, Circuito de la Investigación Científica, 04510 Cd. Universitaria, D.F., Mexico
e-mail: raga@astroscu.unam.mx
[5] Institut d'Estudis Espacials de Catalunya and Instituto de Ciencias del Espacio (CSIC), Edifici Nexus, c/ Gran Capitá 2-4, 08034, Barcelona, Spain
e-mail: torrelles@ieec.fcr.es
[6] Instituto de Astrofísica de Andalucía, CSIC, c/ Sancho Panza s/n, 18008 Granada, Spain
e-mail: lfm@iaa.es
[7] Astronomy Department, University of Manchester, Jodrell Bank, Macclesfield, Cheshire SK11 9DL, UK
[8] Instituto de Astronomía, UNAM, Circuito de la Investigación Científica, 04510 Cd. Universitaria, D.F., Mexico
e-mail: lorenzo@astroscu.unam.mx

Received 28 February 2002 / Accepted 27 March 2002

Abstract. The kinematics and physical conditions of the bipolar planetary nebula M 2-48 are analysed from high and low dispersion long-slit spectra. Previous CCD narrow-band optical observations have suggested that this nebula is mainly formed by a pair of symmetric bow-shocks, an off-center semi-circular shell, and an internal bipolar structure. The bipolar outflow has a complex structure, characterised by a series of shocked regions located between the bright core and the polar tips. There is an apparent kinematic discontinuity between the bright bipolar core and the outer regions. The fragmented ring around the bright bipolar region presents a low expansion velocity and could be associated with ejection in the AGB-PN transition phase, although its nature remains unclear. The chemical abundances of the central region are derived, showing that M 2-48 is a type I planetary nebula (PN).

Key words. ISM: jets and outflows – hydrodynamics – shock waves – planetary nebulae: individual: M 2-48

1. Introduction

The morphology of M 2-48 has been previously discussed by Vázquez et al. (2000) [hereafter Paper I] who found the full extent of its bipolar structure and indications of the presence of high-velocity outflows from their monochromatic images. The occurrence of highly collimated, high velocity jet-like components in planetary nebulae is well established (e.g. Miranda & Solf 1992; López et al. 1995; Sahai & Trauger 1998; Miranda et al. 1999; O'Connor et al. 2000; Miranda et al. 2001; Gonçalves et al. 2001, etc.). These bipolar outflows usually show indications of episodic outburst and rotation or precession of the symmetry axis (e.g. López et al. 1997). The origin of such outflows is intimately related to the formation and shaping of PNe and thus their kinematic characterisation is a key parameter for the models. Several models have been proposed for the generation of collimated outflows in PNe, such as pure hydrodynamical models (Icke et al. 1992; Mellema 1995, 1997), models involving stellar rotation and magnetized winds (Różyczka & Franco 1996; García-Segura 1997; García-Segura & López 2000), and the influence of binary system (Soker & Livio 1994; Reyes-Ruíz & López 1999; Soker 2002).

The bipolar planetary nebula M 2-48 has three main structural components: (1) an internal bipolar central region (CR); (2) an off-center semi-circular fragmented shell, containing a region with a bow-shock morphology (this

Send offprint requests to: L. López-Martín,
e-mail: luis.lopezmartin@obspm.fr

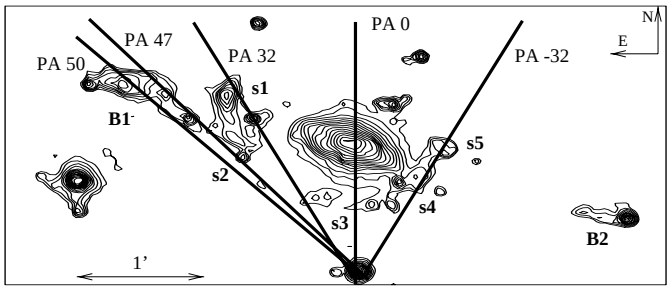

Fig. 1. Slit positions of the low-dispersion spectroscopy are marked over the contour plot of a [N II] 6584 Å CCD image of M 2-48 taken from Vázquez et al. (2000).

has been interpreted in Paper I as the possible interaction of the bipolar, collimated outflow with the shell), and (3) a pair of symmetric knots with a seemingly bow-shock morphology, located at either side at $\approx 2'$ from the center (see Paper I).

In order to analyze the kinematical structure, excitation mechanisms and chemical abundances of M 2-48, spatially resolved high and low dispersion spectroscopy have been now obtained. We first describe the observations and the results extracted from the position-velocity (PV) diagrams in Sect. 2. The kinematical structure and morphology are discussed in Sect. 3, including a simple model to predict the orientation of the shocked structures with respect to the plane of the sky. In Sect. 4, the excitation mechanism and chemical abundances at different regions of the nebula are derived. Finally, our main conclusions are summarized in Sect. 5.

2. Observations and results

Low-dispersion (LD) spectroscopy was obtained in 1999, July 18, 19 and 20, with the B&Ch spectrometer combined with the f/7.5 focus of the 2.1-m OAN telescope at the Sierra de San Pedro Mártir, B. C., Mexico. A 300 lines/mm grating was combined with a 220 μm ($\equiv$2.9 arcsec) slit width and a Tektronix CCD of 1024 $\times$ 1024 pixel, 24 μm square pixels ($\equiv$0.84 arcsec) as detector. The resulting spectra cover from 3400 to 7500 Å, with a 12 Å spectral resolution. The slit was oriented in several position angles (PA) to cover different regions of the PN. Figure 1 shows the slit positions over a contour plot of the [N II] 6584 Å image (Paper I). The LD CCD frames were trimmed, bias-subtracted, flat-fielded and sky-subtracted with standard techniques using IRAF. Flux calibration was performed using sensitivity functions derived from the standard star HD 192281. Table 1 presents the log for each of the 1D spectra that have been extracted and analyzed and Fig. 2 shows the one-dimensional spectra of CR and B1.

The high-dispersion (HD) spectroscopy was obtained in 1999, June 29 and 30, with the Manchester Echelle Spectrometer (MES; Meaburn et al. 1984) combined with the f/7.9 focus at the 2.1-m OAN telescope at the Sierra de San Pedro Mártir, B. C., Mexico. This spectrometer

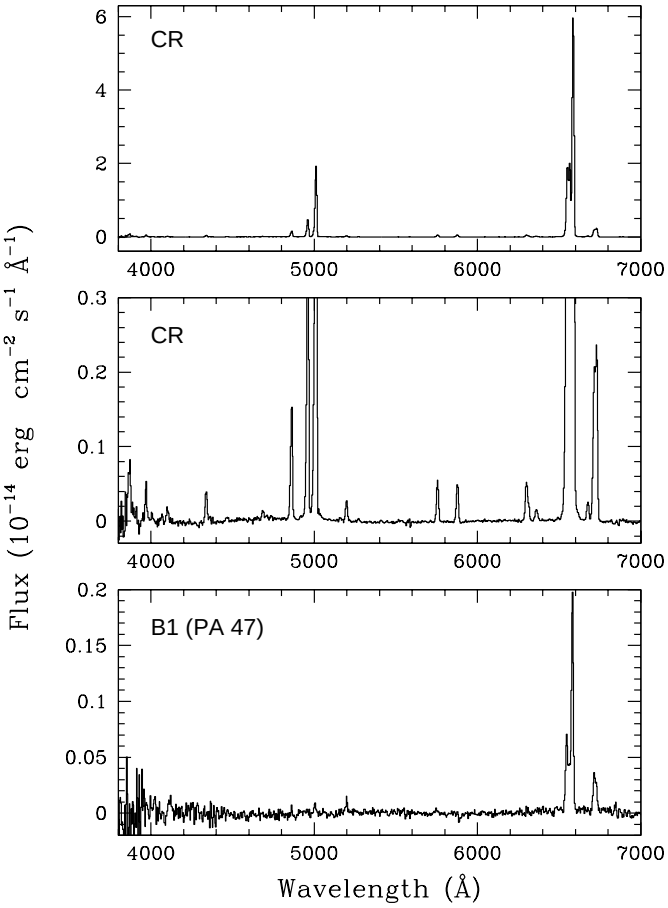

Fig. 2. Low-dispersion optical spectra of two different regions of M 2-48. The central region (CR) is shown expanded along the flux axis in the middle panel. The bow-shock B1 is shown in the bottom panel.

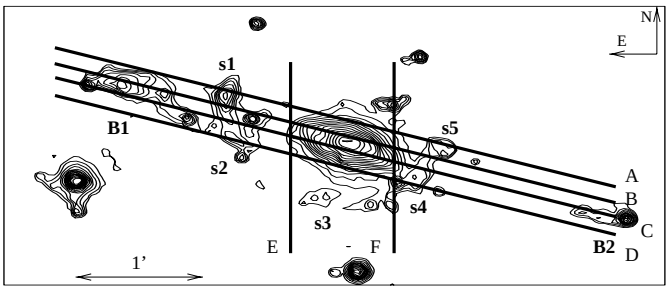

Fig. 3. Slit positions of the high-dispersion spectroscopy (A-F) are marked against a contour plot of a [N II] 6584 Å CCD image of M 2-48 taken from Vázquez et al. (2000).

Table 1. Data of the 1D spectra extracted from the low dispersion spectra.

Region	PA (°)	Exposure time (s)	Slit length (arcsec)
CR	0	3600	25.9
s1	32	2400	11.5
s4	−32	1800	8.6
B1	47	1800	20.2
B1	50	3000	4.8

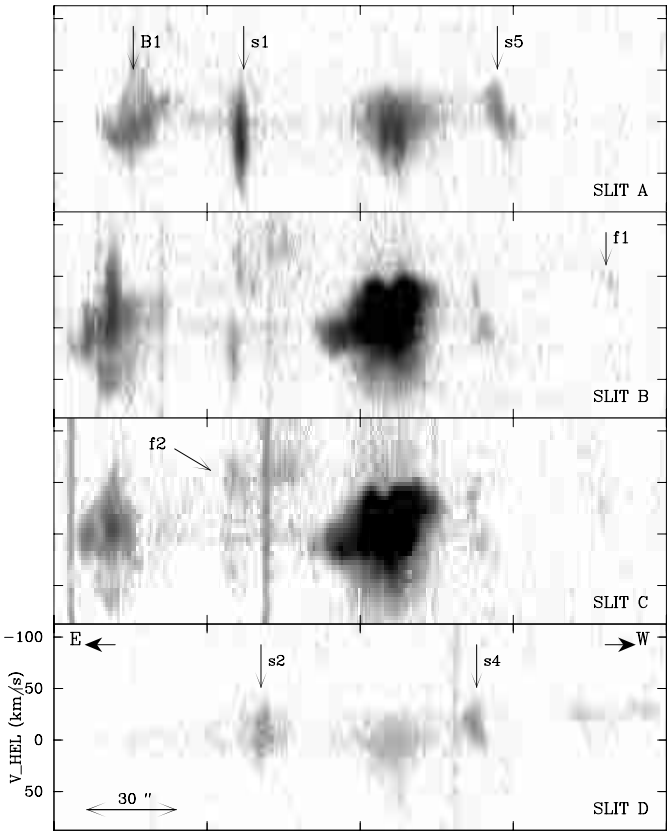

Fig. 4. Gray-scale representation of the position-velocity arrays of [N II] 6584 Å along slits A – D. Labels correspond to the regions indicated in Fig. 3.

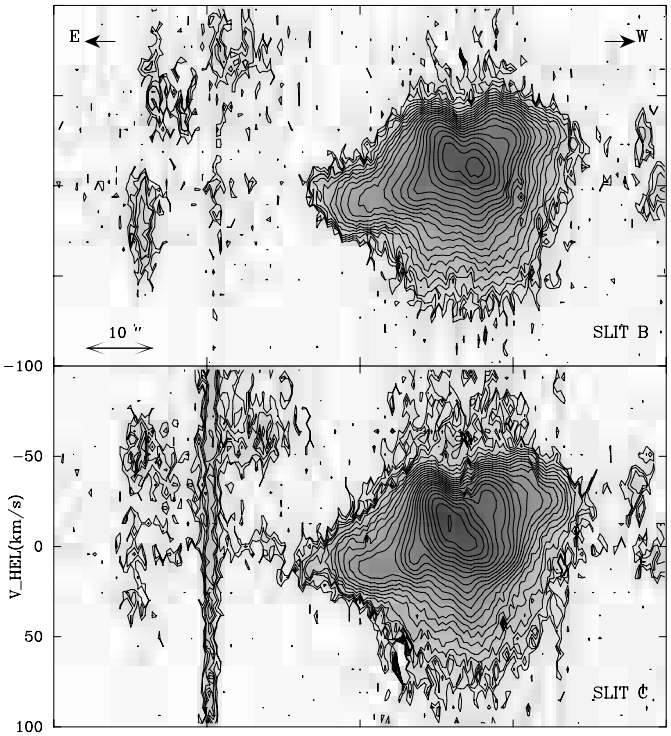

Fig. 5. [N II] 6584 Å PV diagrams of the central region of M 2-48 (for slit positions B and C). The line profiles are shown with a greyscale and overlayed logarithmic contours.

has no cross-dispersion. A 90 Å bandwidth filter was used in order to isolate the 87th order, which contains the Hα and [N II] 6548, 6584 Å emission lines.

A Tektronix CCD with 1024×1024, 24 μm ($\equiv$0.3 arcsec) square pixels was the detector. A 2×2 binning was employed in both spatial and spectral dimensions. The "seeing" varied between 1 and 2 arcsec during the observations. In Fig. 3, the slit positions A-F are shown against a contour plot of [N II] 6584 Å of M 2-48. The 150 μm ($\equiv$1.9 arcsec) wide slit was oriented at a position angle PA = 75° for slits A – D and North-South for slits E – F. The spectral resolution is 10 km s^{-1}. Exposure times of 1800 s were carried out for each slit position. Images were reduced in the standard manner using IRAF. The spectra were wavelength calibrated with a Th-Ar lamp to an accuracy of $\pm$1 km s^{-1}.

The bidimensional arrays of [N II] 6584 Å position-velocity (PV) line profiles from the HD spectra (slits A-D), are shown in Fig. 4. Figures 5–7 show enlargements of the core region for slits B and C; the line profiles from slits E and F and the line profiles at the tip of north eastern lobe for slits B and C, respectively.

3. Morphology and kinematics

M 2-48 has a bipolar morphology, as has been described in Paper I (see also the images in Manchado et al. 1996). From a bright bipolar core emerge relatively faint, broken filaments that delineate fairly tight collimated lobes extending over 2 arcmin on either side. Some of the filaments close to the core seem to trace an incomplete arc that gives the appearance of being the remnants of a spherical shell. The PV diagrams shown in Figs. 4–7 reveal the complex kinematic structure of the main components of M 2-48. The labels B1, s1, s2, s4 and s5 in the PV arrays in Fig. 4 match the location of the regions with the same labels in Fig. 3, where we have followed the nomenclature of Paper I. The spectral element labeled as (f1) is probably related to the tip of the southwestern lobe.

3.1. Central region

Line profiles from the bright nebular core are shown in detail in Fig. 5. The systemic velocity of the core, as defined by the central intensity maximum of the line profiles shown in Fig. 5 lies around -15 km s^{-1}. The line profiles replicate a bipolar outflow emerging from a bright, compact core, extending bluewards to -50 km s^{-1} on the west side and redwards to $+25$ km s^{-1} on the east side. The line profile from slit C (bottom panel in Fig. 5) shows particularly extended wings, reaching remarkable values of $\pm$85 km s^{-1} at *FWZI* within the central ($\sim$20 arcsec) region. The bright compact core itself is seen elongated and tilted in the velocity space, expanding towards negative velocities on the east side (-25 km s^{-1}) and positive velocities on the west side ($+10$ km s^{-1}).

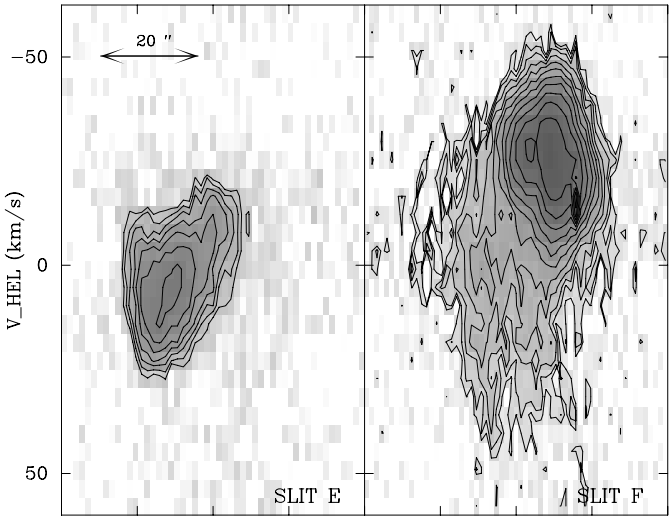

Fig. 6. [N II] 6584 Å PV diagrams of the bipolar lobes of M 2-48 (for slit positions E and F). The line profiles are shown with a greyscale and with logarithmic contours.

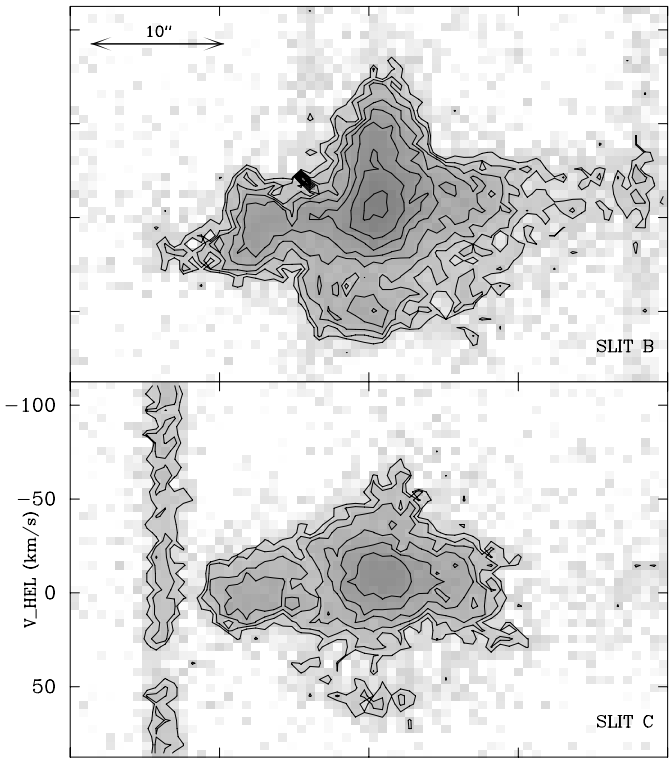

Fig. 7. [N II] 6584 Å PV diagrams of the bow-shock B1 of M 2-48 (for slit positions B and C). The line profiles are shown with a greyscale and with logarithmic contours.

3.2. The arc-like structure

One of the curious features of M 2-48 is a group of several knots around the central bipolar region that seem to form an arc-like structure (Paper I). These knots (s1-s5 in Fig. 1) were interpreted as possible segments of an expanding semi-circular shell. Some slits were obtained with the purpose of intersecting this possible expanding shell and clarify their nature. The line profiles shown in Fig. 6, are found to follow the velocity pattern of the bipolar outflow emerging from the extended regions of the core, with redshifted velocities on the east side ($\approx$+10 km s^{-1}) and blueshifted velocities on the west side ($\approx$−25 km s^{-1}). No indications of a velocity ellipse that could hint to the presence of an expanding shell are detected, at least with the present spectral resolution.

3.3. Bow-shock s1

The eastern lobe is the brighter one, with several high-speed knots with bow-shock-like morphologies being detected in the HD spectra, namely B1, s1 and s2. On the western lobe we detect and identify knots s4 and s5, and the feature f1 (see Figs. 3 and 4).

A high-velocity element, labeled s1 in Fig. 4, coincident with the position of a bright knot on the eastern side and near a portion of the arc-like structure, shows an apparent bow- shock morphology and kinematical structure (see Figs. 3 and 8, bottom right and the image in Manchado et al. 1996). It is of interest to estimate the orientation angle of the bow-shock associated with knot s1 with respect to the plane of the sky, ϕ. To do that, we have used a "3/2-D" model to predict the position-velocity diagram of a bow-shock at different angles with respect to the plane of the sky. Raga & Noriega-Crespo (1993) found that the Hα emission per unit time and area is approximately given by:

$$I_{\mathrm{H}\alpha} \propto (v_{\mathrm{shock}})^{\gamma_{\mathrm{H}\alpha}} , \quad (1)$$

where v_{shock} is the shock velocity and $\gamma_{\mathrm{H}\alpha}$ is a constant dependent on the shock velocity regime.

If we assume that the jet is moving along the z-axis, the shape of the bow-shock can be parametrized by:

$$r \propto z^{p} , \quad (2)$$

where p determines the aperture of the bow-shock. We have used a value of $p = 2$.

Thus, the input parameter for the model essentially is the shock velocity. This velocity can be estimated from the PV diagrams obtained from the long-slit spectroscopy (Fig. 4).

In addition, we use the value of $\gamma_{\mathrm{H}\alpha} = 3.49$ corresponding to the 20.0–81.3 km s^{-1} range of velocities proposed by Raga & Noriega-Crespo (1993).

We can calculate the Hα emission, and predict the position-velocity diagram at different orientations with respect to the sky plane, as shown in Fig. 8. From this comparison we can establish that s1 is inclined at an angle of $\sim$10° with respect to the plane of the sky.

This low inclination angle indicates that the radial velocity of the outflow producing the s1 bow-shock can be a factor of about 6 larger than the velocities derived from the PV diagrams.

We have used the radial velocity of the peak emission of s1, 15 km s^{-1}, as the expansion velocity projected to the line of sight. Using the inclination estimated for s1,

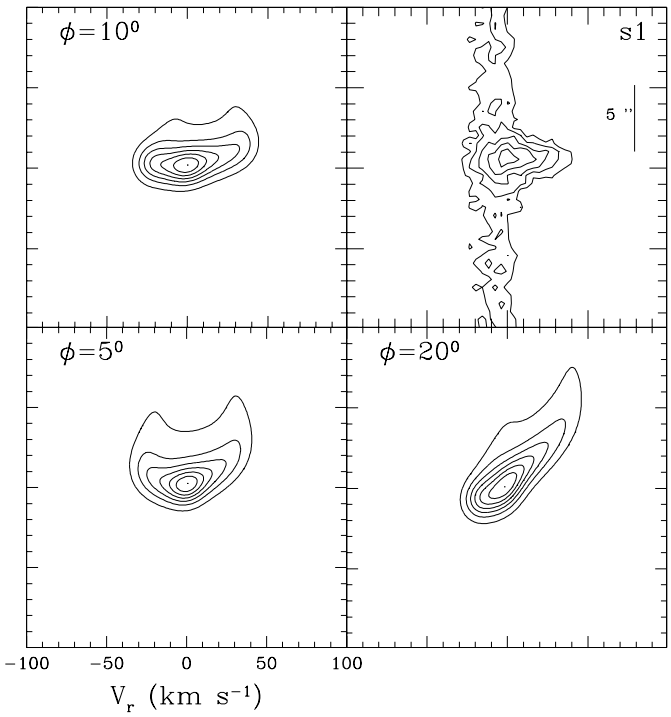

Fig. 8. Comparison of the position-velocity diagram of the s1 bow-shock and "3/2-D" bowshock model fits at different orientations pointing away from the plane of the sky. The best fit is at $\phi = 10^{\circ}$.

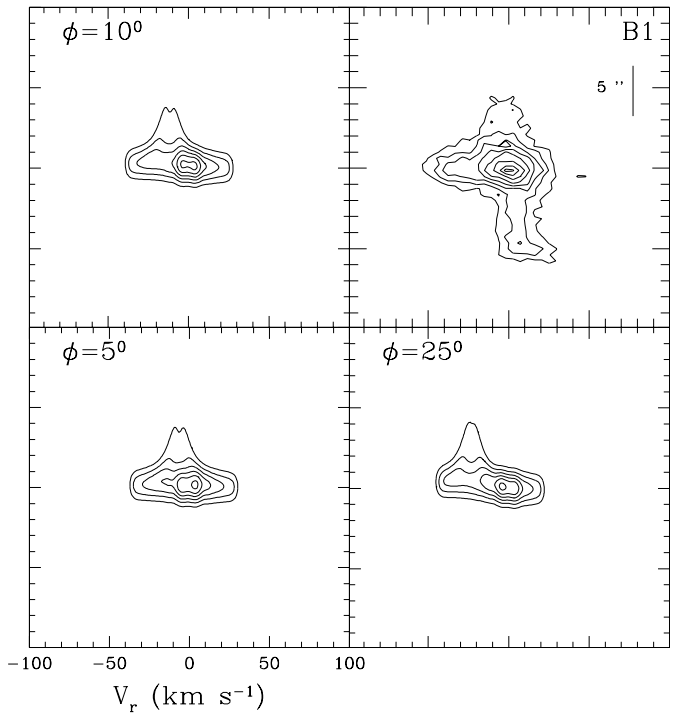

Fig. 9. Comparison of the position-velocity diagram of the B1 bow-shock and "3/2-D" bowshock model fits at different orientations pointing inwards to the plane of the sky. The best fit is at $\phi = 10^{\circ}$.

$\phi \sim 10^{\circ}$, we can determine the tangential expansion velocity. Finally, taking into account the projected linear separation between s1 and the central region we can estimate a dynamical time of $\tau_{s1} \approx 3\,[\mathrm{d/kpc}] \times 10^3$ yr.

In addition, a peculiar feature labelled f2 can be distinguished in the PV diagram of slit C (Fig. 4), with a constant heliocentric velocity of about -60 km s^{-1}. This feature seems to be spatially coincident with the eastern arc, corresponding to the diffuse material between knots s1 and s2.

3.4. External bow-shock B1

In the [N II] 6584 Å direct images (see Paper I), it is possible to see two symmetrical structures with a bow-shock morphology. The eastern knot, B1, which is brighter than the western one, B2, is blueshifted and has a line width of ≈80 km s^{-1}. The PV diagrams of this bow-shock are shown in Fig. 7, where we can see two different zones of B1 covered by the slits B and C. Slit B slightly covers the center of the bow-shock (larger line width), and C covers the wings (smaller line width).

It is possible to use the "3/2-D" model described in Sect. 3.2 to predict the PV diagram of this bow-shock. From the comparison of the observations and the numerical model of the bow-shock B1 for different orientations (see Fig. 9), we can estimate that B1 is inclined at an angle of ∼10° pointing inwards to the plane of the sky. The angle with respect to the plane of the sky suggests that the radial velocity of the bow-shock B1 can be a factor of ≈6 greater than the velocities derived from the PV diagrams. In order to establish a sequence of events, using the same procedure as for s1 (see Sect. 3.3), we estimate the dynamical age of this bow-shock to be $\tau_{B1} \approx 5.3\,[\mathrm{d/kpc}] \times 10^3$ yr. This is consistent with the idea that the bow-shocks B1 and s1 correspond to different bipolar ejections and probably with different axis orientation. This suggests a change in the orientation of the symmetry axis of the successive outflows. In this way, a previous ejection of material would form the expanding arcs interacting with a bipolar outflow and the most external bow-shocks B1 and B2, and a later high-velocity bipolar outflow with different orientation would form the s1 bow-shock.

We have also noted that the symmetry axis of the most internal bipolar region is not coincident with either of these two high-velocity bipolar outflows.

In addition to the main features described in previous sections, we can see other interesting features in the PV diagrams obtained with the HD spectroscopy. In Fig. 4 we can distinguish a very weak feature labelled f1 in slits B and C. This is a component with an heliocentric velocity of ≈−50 km s^{-1}. This emission could correspond to the wing of the western bipolar lobe outflow. Observations at other slit positions or longer exposure times would be necessary to resolve in more detail the kinematical behavior of this feature.

Table 2. Dereddened line intensity ratios.

A - Bright regions

Line	$f(\lambda)$	CR	s1	B1(47°)
3870 He I+[Ne III]	+0.228	107	...	...
3969 H7+[Ne III]	+0.204	51	...	...
4007 [Fe III]	+0.195	9	...	...
4101 Hδ	+0.172	21	...	...
4340 Hγ	+0.129	50	...	...
4363 [O III]	+0.124	9	...	...
4471 He I	+0.095	8	...	...
4686 He II	+0.048	10	...	...
4711 [Ar IV]	+0.036	5	...	...
4740 [Ar IV]	+0.032	3	...	...
4861 Hβ	0.0	100	100	100
4959 [O III]	−0.023	278	...	...
5007 [O III]	−0.024	965	103	172
5152 [Fe III]	−0.064	2	...	...
5198 [N I]	−0.074	15	...	121
5270 [Fe III]	−0.087	2	...	...
5410 He II	−0.116	1	...	...
5755 [N II]	−0.191	16	32	...
5876 He I	−0.216	14	...	...
6300 [O I]+[S III]	−0.285	14	72	...
6364 [O I]	−0.294	4	34	...
6548 [N II]	−0.321	285	214	481
6563 Hα	−0.323	286	275	286
6584 [N II]	−0.326	860	622	1340
6678 He I	−0.338	4	...	...
6717 [S II]	−0.343	29	121	192
6731 [S II]	−0.345	35	95	139
7065 He I	−0.383	4	...	...
7135 [Ar III]	−0.391	25	...	...
7330 [O II]	−0.410	8	...	...
C(Hβ)		1.88	1.82	1.47
I(Hβ)[1]		171	6.0	2.1
N_e([S II])		1260	180	<100
T_e([O III])		10850	...	...
T_e([N II])		10700	20100	...

[1] In units of 10^{-14} erg cm^{-2} s^{-1}.

B - Faint regions

Line	s4 (-32°)	B1(50°)
6548 [N II]	...	122
6563 Hα	100	100
6584 [N II]	82	410
6717+31 [S II]	55	152
$F(\mathrm{H}\alpha)^1_{\mathrm{obs}}$	1.1	0.6

[2] In units of 10^{-15} erg cm^{-2} s^{-1}.

4. Line intensity ratios and chemical abundances

As noted in Sect. 2, five regions were selected from the slit positions observed with low resolution spectroscopy (see Fig. 1), covering the four different morphological zones pointed out in Paper I. In Fig. 2, the flux calibrated spectra of two different zones are shown. The top and middle panels correspond to different scales (high and low

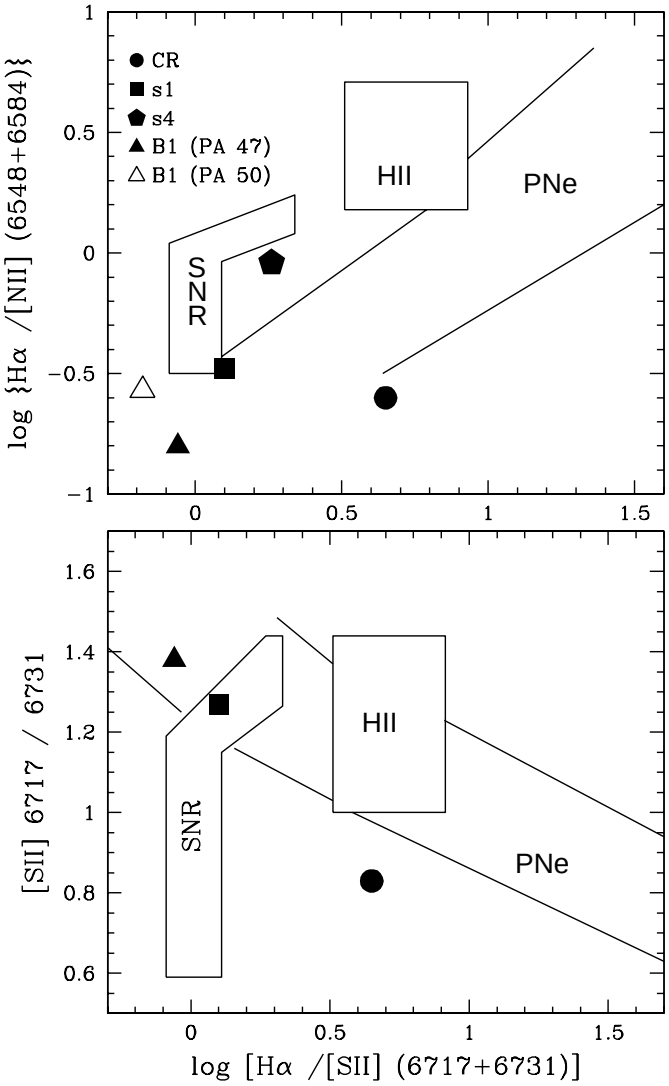

Fig. 10. Diagnostic diagrams showing the emission line ratios of the different regions observed in M 2-48. Top: log Hα/[SII] vs. log Hα/[NII]. Bottom: log Hα/[SII] vs. the electron density indicator [SII] 6717/6731 (adapted from Sabbadin et al. 1977).

Table 3. Chemical abundances in the central region.

12+log O^+/H^+	7.85
12+log O^{++}/H^+	8.43
12+log O/H	8.55
log N^+/O^+	+0.30
12+log Ne^{++}/H^+	7.75
12+log $S^+/^+$	6.16
12+log Ar^{++}/H^+	6.30
12+log Ar^{3+}/H^+	5.77
He^+/H^+ (4471)	0.127
He^+/H^+ (5876)	0.098
He^+/H^+ (6678)	0.096
He^+/H^+ (7065)	0.163
$<He^+/H^+>$	0.100
He^{++}/H^+	0.008
He/H	0.108

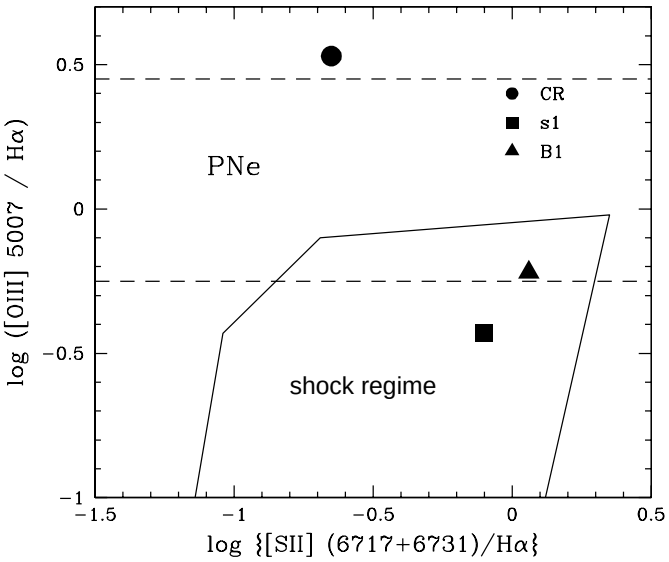

Fig. 11. Diagnostic diagram representing log [SII]/Hα vs. log [OIII]/Hα of the different regions observed in M 2-48 (adapted from Phillips & Cuesta 1999).

intensities, respectively) of the spectrum of the central region. The bottom panel corresponds to the spectrum of B1 (PA 47°).

The extinction coefficient, $C(\mathrm{H}\beta)$, was derived for three regions: Central Region (CR), s1 and B1 (PA 47°) from the comparison of observed and theoretical Hα/Hβ ratios. We have used the calculations of Storey & Hummer (1995) assuming case B and an iteration procedure adopting finally the electron densities (N_e) derived for each particular zone and the electron temperature (T_e) obtained for CR (T_e = 10 800 K) for all of the regions. The reddening law of Seaton (1979) has been used. Dereddened line intensity ratios with respect to Hβ as well as the values of $C(\mathrm{H}\beta)$ for these regions are presented in Table 2. The uncertainties in the line fluxes are of the order of 5% for the brighter lines and about 20–30% for the weaker ones. Emission line fluxes of blended lines such as the Hα+[N II] nebular lines and the [S II] doublet have been obtained from Gaussian fitting of the line profiles using the Starlink DIPSO package (Howarth & Murray 1990). The dereddened, integrated Hβ flux of each region is also included in Table 2.

N_e and T_e (see Table 2) have been derived following standard methods of collisionally excited line ratios using the five-level program for the analysis of emission-line nebulae of Shaw & Dufour (1995). There seems to be a gradient in N_e, with parameter decreasing values towards the external zones. This is consistent with the expansion of stellar ejecta as the distance towards the nucleus increases. T_e derived from [O III] and [N II] lines for CR are almost coincident, indicating that there is no strong temperature stratification in the bright bipolar nebular core of the nebula. The T_e derived for s1 seems too high to be accounted for by pure photoionization, confirming contamination by shock emission in this zone, which morphologically and kinematically resembles a bow-shock (see Sect. 3.3).

The spectra of the other two zones: s4 and B1 (PA 50°), are so faint that Hβ is not measured and therefore it is not possible to derive the extinction coefficient for these regions. The emission line ratios with respect Hβ and the uncorrected Hα flux for these regions are included in Table 2.

We have used several diagnostic diagrams in order to evaluate which is the dominant excitation mechanism prevalent in these regions. In Fig. 10 we show two diagrams involving the locus of several line ratios: Hα/[N II], Hα/[S II], and [S II] 6717/6731 for H II regions, PNe and supernova remnants (adapted from Sabbadin et al. 1977). These diagrams clearly indicate that CR is mainly radiatively excited. However, the positions of s1 and B1 are not so definite, in the sense that some shock contribution is present. The fact that the positions of B1 and s1 are just below the locus of the SNRs in the upper pannel of Fig. 10 could be also due to the high N enrichment of the nebula (see below).

In Fig. 11 we show a diagram adapted from Phillips & Cuesta (1999) involving [O III]/Hα and [S II]/Hα. This diagram includes the locus of the observed emission line ratios for a large number of radiatively excited PNe and predictions from plane-parallel and bow-shock models by Hartigan et al. (1987) and Shull & McKee (1979). The position of the different regions of M 2-48 in this diagram confirms that CR is radiatively excited and that shock excitation is contributing to the spectra of s1 and B1. Assuming purely shock excitation for these zones and comparing their line intensities with the models by Hartigan et al. (1987) we find the best agreement for models with shock velocities of 60 and 130 km s^{-1}, respectively, in agreement with the values obtained in previous sections.

Ionic abundances of the CR are shown in Table 3 and have been derived using the emission line ratios given in Table 2, the code of Shaw & Dufour (1995), and assuming T_e = 10 800 K and N_e = 1260 cm^{-3}. To derive the $\mathrm{He}^+/\mathrm{H}^+$ and $\mathrm{He}^{++}/\mathrm{H}^+$ ratios we have used the effective recombination coefficients given by Péquignot et al. (1991) for all the lines involved. The He^+ abundances obtained from each individual line have been corrected for collisional contributions following Kingdon & Ferland (1995). The final, adopted value of the He^+ abundance is the average of the values obtained for the different individual lines excluding HeI 7065 Å, which suffers from the largest collisional effects.

The total O abundance has been determined from the derived abundance of O^+ and O^{++} combined with the ionization correction factor (ICF) for the presence of O^{3+} proposed by Kingsburgh & Barlow (1994). The total He/H ratio has been obtained simply by adding the $<\mathrm{He}^+/\mathrm{H}^+>$ and $\mathrm{He}^{++}/\mathrm{H}^+$ ratios.

The $\log \mathrm{N}^+/\mathrm{O}^+ = +0.30$ obtained for the nebula clearly indicates that it is a nitrogen-enriched object. Taking into account the chemical classification proposed by Peimbert & Torres-Peimbert (1987), M 2-48 should be classified as a type I PN ($\log \mathrm{N/O} \geq -0.30$ and/or

He/H $\geq$ 0.125), although it is not a helium-rich object. The O/H ratio is slightly lower than the average of the Galactic Type I PNe (12+log O/H = 8.65, Kingsburgh & Barlow 1994).

5. Conclusions

The kinematic mapping of M 2-48 has revealed a complex bipolar structure characterised by a series of shocked regions extending accross the major axis of the nebula and reaching the tips found in Paper I. Indications that the bipolar outflow has suffered some changes in direction have also been detected. 3/2 D shock models of the line profiles are consistent with the main bipolar outflow having a small $\pm 10^{\circ}$ angle with respect to the plane of the sky, thus making the real outflow velocity some six times larger than the observed one. The line fluxes derived from the low dispersion spectrum in the central region show that M 2-48 is nitrogen enriched; and should be classified as type I.

Acknowledgements. We would like to thank the referee, You Hua Chu, for useful comments that improved our paper. López-Martín is grateful for the receipt of a graduate scholarship from DGEP-UNAM (México). López-Martín and Raga acknowledge support from the CONACyT grant 34566-E. J. A. López ackowledges support from CONACYT and DGAPA (UNAM) through projects 32214-E and IN114199. Vázquez was partially supported by the CONACyT grant I32815E. Miranda and Torrelles acknowledge support from DGESIC grant PB98-0670-C02, and from Junta de Andalucía (Spain). Olguín is grateful for the receipt of a graduate scholarship from DGAPA-UNAM (México). We thank R. Cook and the SPM staff for help during the observations.

References

García-Segura, G. 1997, ApJ, 489, L189
García-Segura, G., & López, J. A. 2000, ApJ, 544, 336
Gonçalves, D. R., Corradi, R. L. M., & Mampaso, A. 2001, ApJ, 547, 302
Hartigan, P., Raymond, J., & Hartmann, L. 1987, ApJ, 316, 323
Howarth, I. D., & Murray, J. 1990, SERC Starlink User Note, No. 50
Icke, V., Balick, B., & Adam, F. 1992, ApJ, 253, 224
Kingdon, J. B., & Ferland, G. J. 1995, ApJ, 442, 714
Kingsburgh, R. L., & Barlow, M. J. 1994, MNRAS, 271, 257
López, J. A., Vázquez, R., & Rodríguez, L. F. 1995, ApJ, 455, L63
López, J. A., Meaburn, J., Bryce, M., & Rodríguez, L. F. 1997, ApJ, 475, 705
Manchado, A., Guerrero, M. A., Stanghellini, L., & Serra-Ricart, M. 1996, The IAC Morphological Catalog of Northern Galactic Planetary Nebulae (La Laguna: IAC)
Meaburn, J., Blundell, B., Carling, R., et al. 1984, MNRAS, 210, 463
Mellema, G. 1997, A&A, 321, 29
Mellema, G. 1995, MNRAS, 277, 173
Miranda, L. F., & Solf, J. 1992, A&A, 260, 397
Miranda, L. F., Guerrero, M. A., & Torrelles, J. M. 1999, AJ, 117, 1421
Miranda, L. F., Guerrero, M. A., & Torrelles, J. M. 2001, MNRAS, 322, 195
O'Connor, J. A., Redman, M. P., Holloway, A. J., et al. 2000, ApJ, 531, 336
Peimbert, M., & Torres-Peimbert, S. 1987, RMxAA, 14, 540
Péquignot, D., Petitjean, P., & Boisson, C. 1991, A&A, 251, 680
Phillips, J. P., & Cuesta, L. 1999, AJ, 118, 2919
Raga, A. C., & Noriega-Crespo, A. 1993, RMxAA, 25, 149
Reyes-Ruiz, M., & López, J. A. 1999, ApJ, 524, 952
Różyczka, M., & Franco, J. 1996, ApJ, 469, L130
Sabbadin, F., Minello, S., & Bianchini, A. 1977, A&A, 60, 147
Sahai, R., & Trauger, J. T. 1998, ApJ, 1357
Seaton, M. J. 1979, MNRAS, 187, 73
Shaw, R. A., & Dufour, R. J. 1995, PASP, 107, 896
Shull, J. M., & McKee, C. F. 1979, ApJ, 227, 131
Soker, N. 2002, in press [astro-ph/0107554]
Soker, N., & Livio, M. 1994, ApJ, 421, 219
Storey, P. J., & Hummer, D. G. 1995, MNRAS, 272, 41
Vázquez, R., López-Martín, L., Miranda, L. F., et al. 2000, A&A, 357, 1031 (Paper I)